

Fabrication of AZ31/ZnO surface composite by friction stir processing: Evolution of microstructure, mechanical properties and corrosion behavior

Huda H. Zamel¹, Al-Ezzi Salih^{1*} , Muna Khethier Abbass², Hanaa Soliman³, Ying Zeng⁴

¹ Engineering Technical College Baghdad, Middle Technical University (MTU), 10047, Baghdad, Iraq

² Production Engineering and Metallurgy Department, University of Technology, 10069, Baghdad, Iraq

³ Central Metallurgical Research and Development Institute, CMRDI, Helwan, 11421, Cairo, Egypt

⁴ Key Laboratory of Advanced Technologies of Materials, Ministry of Education, School of Material Science and Engineering, Southwest Jiaotong University, Chengdu 610031, China

* Corresponding author's e-mail: alezzisalih@mtu.edu.iq

ABSTRACT

In this research, the surface of magnesium alloy AZ31 is modified by friction stir processing (FSP). The modification process consists of synthesis AZ31/ZnO composite by establishing holes at surface which are filled with nano ZnO and FSP was carried out at traverse speed 45 mm/ min. and rotational speed of 1100 rpm. Nano ZnO is a biocompatible material and it was used previously for coating AZ31 alloy in lightweight industrial applications. However, the novel surface composite of AZ31/ZnO established in solid-state processing (FSP). The results show that the corrosion product layer has increased passivity at the modified surface which exhibited lower corrosion rate (51%) than that of base alloy AZ31, due to the presence of nano ZnO particles. On the other hand; the hardness increased which can be attributed to the grains refinement (from 15 to 4.3 μm) and the formation of nanocomposite at the surface. The research shows a promise in lab-based studies, that can be a way to manufacture large-scale biomaterials.

Keywords: AZ31/ZnO, surface nanocomposites, friction stir processing, grain refinement, hardness, corrosion rate.

INTRODUCTION

Magnesium alloys offer attractive materials with high specific strength, lightweight, good castability, machinability [1], damping properties, biocompatibility [2], and biodegradability [3] in addition to many uses in the automotive, aerospace, electronics, biomedical [4], and recreational industries [5] due to their relatively strong electrochemical activity in an aqueous environment. Magnesium alloys are mostly limited in engineering and biomedical applications, where they might experience severe corrosion rates and mechanical property loss [6]. These applications frequently call for high strength, hard, and wear resistance components, which metal matrix composites (MMCs) may successfully meet [7]. Selecting the proper reinforcing and fabrication

technique is essential. Using magnesium alloy components to manufacture a surface-reinforced composite has proven to be a significant difficulty. Various surface modification techniques have been developed for Mg alloys. High-temperature, liquid-state techniques including laser surface engineering[8], high-energy electron beam irradiation[9], thermal spraying [10], cast sinter [11], and gas tungsten arc treatment [12] have all been used to modify alloy surfaces. It is reasonable to use surface treatment techniques in a solid form in this situation. One method of treating solid-state surfaces is friction stir processing (FSP). This process has several advantages, including as uniformity, enhanced microstructure, solid-state processing, and being an energy and environmentally-friendly way [13–17]. Numerous research studies on the FSP of the magnesium alloy

AZ31 have addressed the creation of various surface composite types as well as the evolution of the microstructure and biodegradation in simulated body fluid (SBF) [18, 19]. Morrisada et al. [20] distributed micro SiC particles by FSP in the AZ31 Mg alloy matrix and demonstrated how the SiC particles stabilize the microstructure at high temperatures (~400 °C), improve hardness, and refine the grains. Chang et al. [21] stated that FSP can be used to get the ultra-fine grain (UFG) structure of the AZ31 Mg alloy. Azizieh et al. [22] AZ31/Al₂O₃ surface composite was created by FSP, and the influence of pin profile and rotational tool speed on the development of microstructure and particle dispersion was examined. Chang et al. [21] used FSP to create AZ31/SiO₂ and AZ31/ZrO₂ nanocomposites, and the results demonstrate a notable improvement in the hardness and tensile characteristics. The results demonstrated that; an increasing of the maximum shear strain rate may also be achieved by FSP-adding ZrO₂ nanoparticles to the AZ31 substrate. Additionally, the corrosion performance of the AZ series of magnesium alloys was enhanced by FSP. According to Liu et al. [23] concluded that, the FSP can enhance the corrosion behavior of the AZ91 Mg alloy in an aqueous solution containing 3.5wt % NaCl. This is because the corrosion product layer has increased passivity [23]. Abbasi et al. [24] created surface nanocomposites on the AZ91 Mg alloy reinforced with Al₂O₃ and SiC nanopowders using four FSP passes, which improved the nanocomposites' resistance to corrosion. It has been found that adding SiC particles to the FS welded zones of AZ31 magnesium alloy sheets during friction stirring improved their resistance to corrosion [25]. The effects of FSP pass number on the AZ91/Al₂O₃ and AZ91/SiC surface composites were studied by Asadi et al. [26]. It was demonstrated that several aspects of the composites, including hardness and tensile behavior, improved after eight FSP passes. Additionally, they demonstrated that the removal of reinforcing powder microclusters only requires four FSP passes [26]. Other studies have looked into how FSP affects the tribology behavior of the magnesium alloy AZ31 [27]. Moreover, ZnO NPs are believed to be nontoxic, bio-safe, anti-inflammation, biocompatible, and anti-bacterial. ZnO is an excellent option for anticorrosive additive protection of magnesium alloys since it is inexpensive, and has high stability. Among the published reports, the first effort

to include ZnO nanoparticles (NPs) into plasma electron oxidation (PEO) coatings was conducted on AZ31 Mg alloy and pure aluminum (Al) substrate. The results showed that adding ZnO NPs improved the photoactivity of MgO and Al₂O₃ coatings, respectively [28, 29]. Roknian et al. [30] showed that the PEO-coated sample with a greater ZnO NP content had a stronger antibacterial effect. ZnO particles have also been utilized in cosmetics, fillers for medicinal products, and medication carriers [31]. More recently, it has been shown that ZnO can improve osteoblast development, adhesion, and proliferation in bone composites [32].

From literature reviews and studies, this study attempts to incorporate ZnO NPs and AZ31 alloy. The proposed novel MMC consists the both metal and ceramic biocompatible AZ31 and ZnO with hexagonal crystal structures. Then investigates the effect of NP's on the microstructure, mechanical properties, and corrosion behavior. FSP technique, proposed to establish AZ31/ZnO surface nanocomposite by introducing the synergistic qualities of stable ZnO into the magnesium alloy AZ31.

EXPERIMENTAL WORK

Materials

Metal sheets of AZ31 magnesium alloy (100 × 80 × 5 mm³) and the ZnO powders were the materials utilized in this study as a reinforcement for producing an AZ31/ZnO surface nanocomposite. The ZnO powder has 99% purity and a nanorods shape. A quantometer analysis was employed to obtain the chemical compositions of the AZ31 as shown in Table 1.

FSP processing procedure

According to many previous studies, the traverse speed of 45 mm/min, rotational speed of 1100 rpm, the traditional cylindrical threaded pin H13 steel tool (pin diameter 6mm, shoulder diameter 18 mm) and tilt angle of 2° are selected [33, 34]. During processing via FSP, the net design as a zig-zag of 32 holes (2 mm diameter, 2 mm depth, and 2 mm step) was used to compact the ZnO into the alloy matrix AZ31 (Figure 1). This technique is proposed to be effective in dispersing and inhibiting the agglomeration of the nanoparticles [30, 35, 36].

Table 1. Chemical compositions of the magnesium alloy AZ31

Element wt.%	Cu	Zn	Al	Mn	Si	Mg
Measured	0.0020	1.15	2.77	0.374	0.0005	Balance
Standard	0.05	0.8-1.4	2.40-3.60	0.35	0.1	Balance

The weight percent of the nanoparticle were estimated as given in Equation 1:

$$W_{ZnO}\% = \frac{V_h \times \rho_{ZnO}}{(V_m \times \rho_{Mg}) + (V_h \times \rho_{ZnO})} \quad (1)$$

where: $W_{ZnO}\%$ is the reinforcement percent, V_h is the volume of 32 holes with a diameter of 2 mm for each of them, ρ_{ZnO} density of nanoparticles (5.6 g/cm³), V_m is the volume of the matrix and ρ_{Mg} density of AZ31 (1.77 g/cm³).

The estimated ZnO is 36 wt% (16 vol.%). It should be mentioned that these estimates provide the optimal percentages for the weight and density of the matrix. While the all values, however, are lower. This finding is explained by the porosity that exists between the particles [30, 35].

One pass of FSP using a pin-less tool was carried out to seal the surface holes which are filled with nano ZnO. Figure 5 illustrates the conceptual framework for creating the AZ31/ZnO surface nanocomposites. Four samples, as received AZ31 base metal (BM), one passes FSPed of BM (1 Pass), two passes FSPed of BM (2 Pass), and two passes FSPed AZ31/ZnO nanocomposite (AZ31/ZnO), are taken into consideration for the investigation.

CHARACTERIZATION

X-ray diffraction (XRD-6000 Shimadzu, Japan) was used to characterize the phases in AZ31 alloy and AZ31/ZnO composite in the 10–80° range. The metallography character development of the microstructure, fracture morphology, and corrosion surface using optical microscopy (OPTIKA IM-3ME, Italy), the (YAXUN YX-AK36) for macroscopy, and the Quanta FEG scanning electron microscope (SEM) (INSPECT F50) equipped with an energy dispersive spectroscope (EDS). All microstructures had their observation surfaces polished and etched utilizing a picric acid solution of 2.1 g of picric acid, 5 mL of acetic acid, 5 mL of distilled water, and 50 mL of ethyl alcohol. Vickers hardness has been determined using a 100 g for 15 second dwell time. On the polished cross-sectional surface of each substance, nine tests have been performed and the hardness results were averaged. The universal tension machine (LARYEE –UE3450; Hong Kong, China) was used for the uniaxial tensile testing. The starting strain rate was 10⁻³ s⁻¹ for the tensile specimens (6 × 4 mm cross-section area); the gauge length was parallel to the FSP direction.

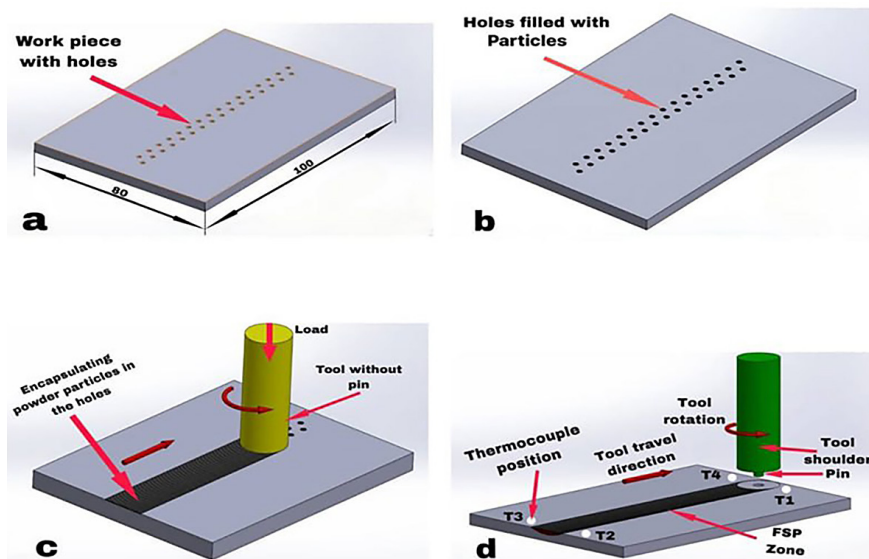


Figure 1. FSP processing of AZ31/ZnO nanocomposite with FSP tools (a) drilling holes (b) holes filled with the ceramics particles (c) closed holes with a pinless tool (d) FSP pin-tool with a thermocouple

For the corrosion test, the electrochemical measurement used a three-electrode electrochemical apparatus that had a fiberglass cell with a 10 mm diameter hole in it. Following ASTM G102-89, the corrosion performance was examined using the (PARSTAT 2273) corrosion instrument for measurement of initial and final potentials, which were held at -2 V and -0.5 V, respectively. The corrosion test samples (AZ31, 1 pass FSP, 2 pass FSP, and AZ31/ZnO) were cut and subsequently ground to create the corrosion specimens. The final stage of preparing the specimens was a thorough cleaning. After that, the samples were placed in a corrosion cell that had an aqueous solution containing 3.5 wt% NaCl. The specimen was utilized as a functioning electrode, and graphite rod (counter electrode) and Ag/AgCl (reference electrode) [37].

RESULTS AND DISCUSSION

Microstructure and grain refinement

Figure 2a shows the macrostructure of the cross-section of the friction stir processed (FSPed) of AZ31/ZnO composite. The onion-like layers of ZnO with the alloy surface are clear. Figure 2 b-e shows the microstructure of the stir zone (SZ), thermomechanical affected zone (TMAZ), and heat affected zone (HAZ) in addition to the base metal (BM). The grain refinement

was achieved at SZ and TMAZ. Furthermore, the grains in HAZ were refined due to the dynamic recrystallization (DRX) when the temperature increased to 400 °C during the heat generation in friction processing as shown in Figure 2f [38, 39]. The increase in temperature higher than the recrystallization temperature (200 °C) was recorded, as shown in Figure 2h. Zhang, Jialong, et al. results [40] show that fine DRX grains appear at the original grain boundaries after hot rolling of AZ31 and the hardness increased due to the decrease of grain size. Niu [41] assumed that the hot deformation mechanism of AZ31 magnesium alloy is primarily continuous DRX. So, it can be suggested that, the fine grains at SZ, TMAZ, and HAZ are formed by DRX of AZ31 during the high strain rate and the generation of high temperature at the surface of the tool in FSP. FSP contributed to the motion and accumulation of dislocations to the grain boundaries which enhanced the DRX of AZ31/ZnO composite. These results are in agreement with other researchers [39, 40, 42], they were fabricated surface composites of AZ61, AZ31 and AA6061 respectively by FSP.

Figure 3 shows the microstructure of the AZ31, friction stir processed (FSPed) AZ31 (1 pass, 2 pass) and AZ31/ZnO composites. As shown in Figure 3(a) the grain size of an extruded plate is 15 μm. The grain size continuously decreased with the increase of friction processing passes as illustrated in Figure 3(b, c). Furthermore, a reduction in grain size was achieved (4.3

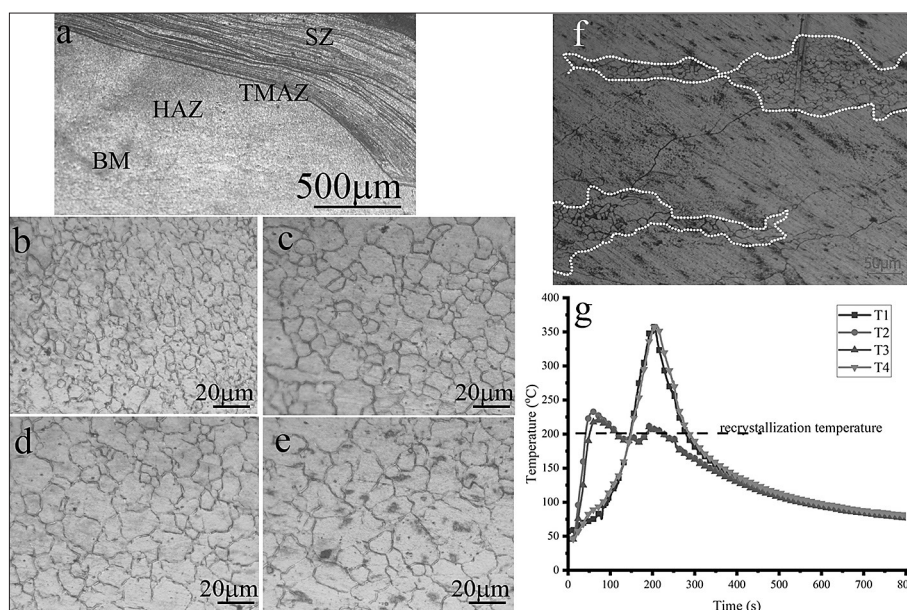


Figure 2. The macro/microstructure of different locations of processed AZ31/ZnO (a) macrostructure of FSPed AZ31/ZnO (b)SZ, (c) TMAZ, (d) HAZ, (e) BM, (h) recrystallization at HAZ, (g) recorded temperature during FSP

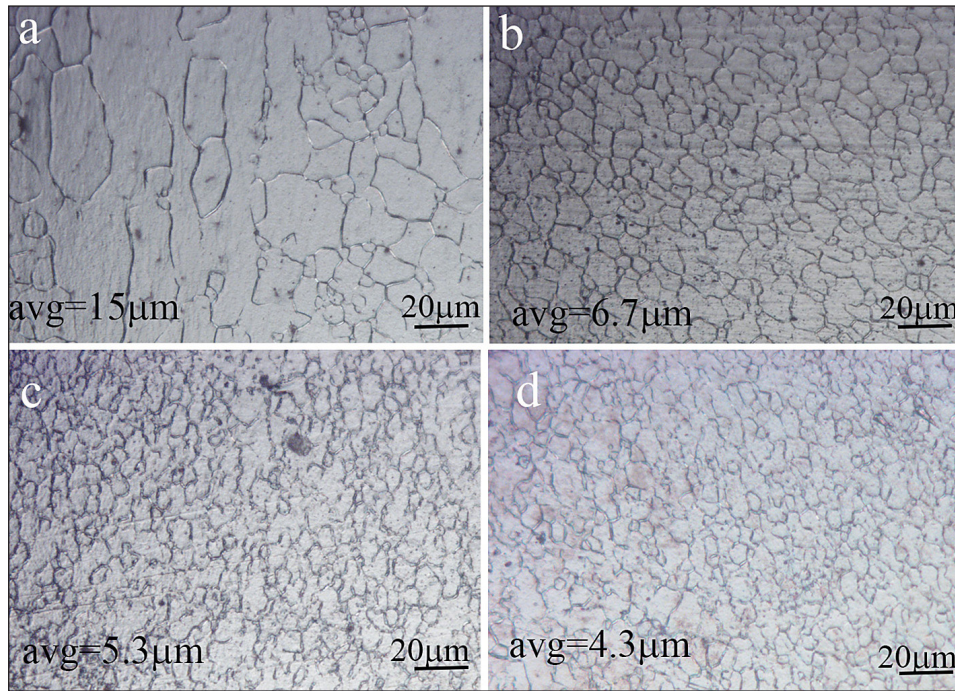


Figure 3. Comparing the grain size and the microstructure of (a) AZ31 Mg alloy matrix, (b) 1 pass FSPed AZ31 (c) 2 pass FSPed AZ31, and(d) AZ31/ZnO processed via 2 pass FSP

µm) with the addition of nano ZnO to the surface as shown in Figure 3(d). Figure 4 (a-c) demonstrates the microstructure and the distribution of magnesium and zinc in AZ31. The uniform distribution of zinc of matrix substrate and nano ZnO within the microstructure of AZ31 are shown in Figure 4(d-f) where the pin and shoulder distributed the nanoparticles by 2 passes. The small agglomeration (weight arrow) of ZnO (Figure 4f) would not only decrease the grain refinement

effect but also deteriorate the tensile strength of the AZ31/ZnO composite.

In addition, the presence of the ZnO phase in the composites was confirmed by the XRD patterns of AZ31/ZnO nanocomposites as shown in Figure 5. The β -Mg₁₇Al₁₂ phase was observed in small amounts distributed in the α -Mg matrix as a small dark spot which was detected in all samples, the particles of ZnO in the prepared composite were identified.

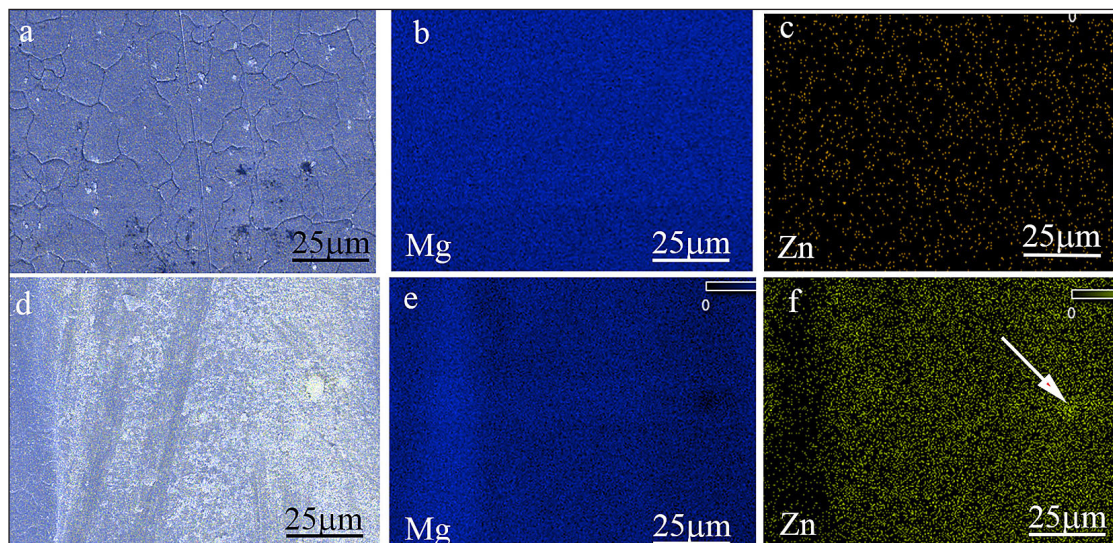


Figure 4. FESEM and EDS mapping of AZ31 and AZ31/ZnO composite (a, b, c) microstructure and distribution of Mg, Zn in as extruded AZ31, (d,e,f) microstructure and distribution of Mg, Zn in AZ31/ZnO composite, respectively

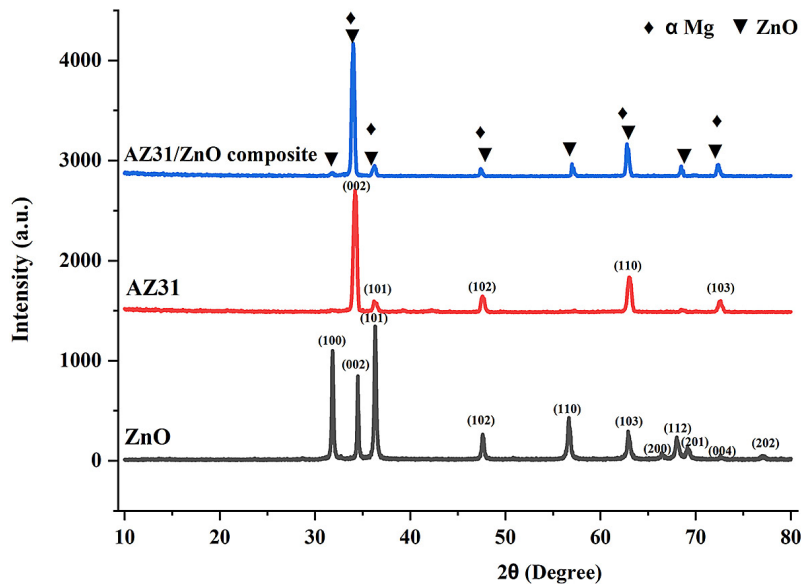


Figure 5. XRD analysis of Nano ZnO, base alloy AZ31, and the prepared composite AZ31/ZnO

Corrosion behavior

It is well known that the corrosion resistance can be improved by grain refinement according to the Hall-Petch formula just like the hardness and tensile strength. Figure 6 illustrates the

Tafel corrosion performance at room temperature for the AZ31 (BM) and FSPed alloy of (1 pass and 2 passes), and AZ31/ZnO composite in a 3.5 wt.% NaCl aqueous solution. According to the extrapolated cathodic Tafel region method, the calculated corrosion potential, and corrosion

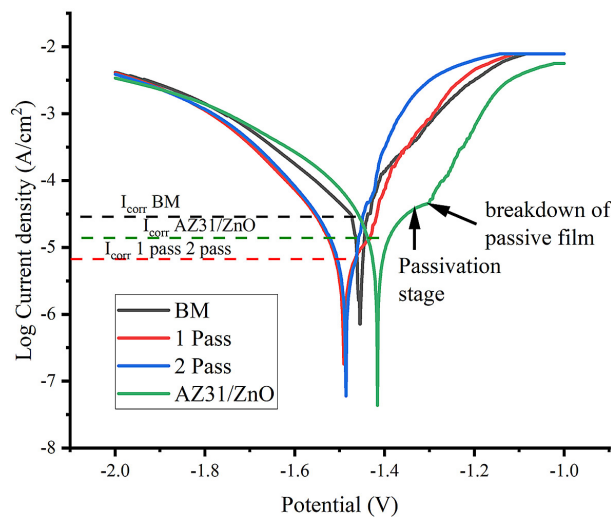


Figure 6. Tafel polarization curve for BM, FSPed sample with 1 pass and 2 pass, and AZ31/ZnO

Table 2. The parameters derived from Tafel polarization curve and the corrosion rate of processed AZ31 and AZ31/ZnO composite

Metal	E_{corr} (V)	I_{corr} ($\mu A/cm^2$)	β_a V/decade	β_c V/decade	CR (mmpy)
AZ31	-1.395	106.992	17.2	-5.59	2.42
AZ31 1 Pass	-1.488	26.818	28.8	-9.10	0.61
AZ31 2 Pass	-1.493	27.434	19.5	-8.74	0.62
AZ31/ZnO	-1.416	52.442	45.4	-8.15	1.18

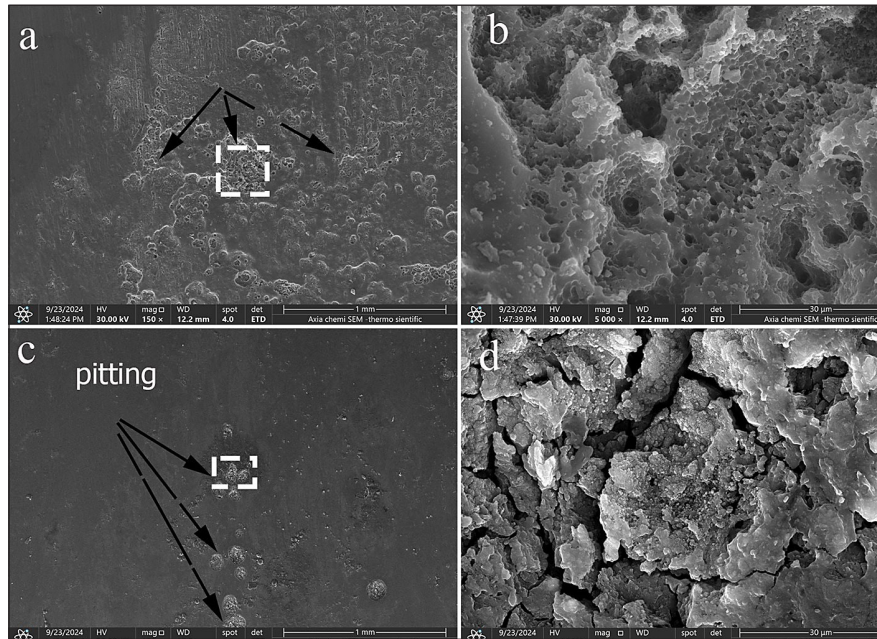


Figure 7. SEM of the surface of the samples after corrosion test (a, b) the surface of BM, (c, d) the surface of AZ31/ZnO composite

current are summarized in Table 2. The corrosion rates (*mmpy*) after the end of the corrosion test were calculated by an equation referred to ASTM G102-89 [43].

$$CR(mmpy) = 3.27 \times 10^{-3} \times I_{corr} \times [EW/\rho] \quad (2)$$

where: *CR* – Corrosion rate in (*mmpy*) unit, I_{corr} – corrosion current density ($\mu A/cm^2$), *EW* – equivalent weight of Mg alloy, which is the atomic weight (24.305) divided by the valance of electrons(2) required to oxidizes Mg, and ρ – density of alloy (1.77 g/cm^3).

The BM recorded a higher I_{corr} , while the FSPed sample shows a lower I_{corr} due to the grain refinement for 1 pass and 2 pass of FSP. The corrosion rate decreased 75% comparing to BM. Although the AZ31/ZnO composite was achieved by 2 passes of the process; the I_{corr} is slightly increased and the corrosion rate increased comparing to 1 pass and 2 pass samples. But the corrosion rate is less than the base metal and decreased 51%. In addition, the Tafel curved moved to the higher potential -1.41V and thus the practical corrosion rate may decrease. S. Jayasathyakawin et al. [44] concluded that 9% ZnO in Mg-3Al MMC increased the corrosion resistance, when the results showed that ZnO decreased the corrosion rate to ~20% of the centered matrix out of ZnO. Corrosion test and surface investigation of the samples exhibit an excellent corrosion

resistance of AZ31/ZnO composite. Figure 7 (a, b) demonstrates the deterioration of the BM and the formation of wide and deep pitting. While the AZ31/ZnO surface composite shows a better corrosion resistance and the formation of the passive film ($Mg(OH)_2$) as shown in Figure 7c-d; which breaks down at -1.32 V.

The grain boundary acts as a physical corrosion barrier. Small grain size creates more grain boundaries, as a consequence, the rate of corrosion in small-grained microstructure slowed down compared with coarse-grained microstructure[37] resulting in relatively more resistance in corrosion. Due to the less physical barrier, coarse-grained microstructure led to an increase in the corrosion rate of the base metal sample. Its corrosion rate was about 4 times higher than that of other AZ31 FSP samples. The corroded surface sample clearly showed how serious of pit formation was within the grains [45, 46]. Also, a protective passive layer was formed for the samples 1 pass, 2 passes, and BM.

Mechanical properties

Hardness and tensile properties

Figure 8 illustrates the average recorded Vickers hardness values of the AZ31 alloy, FSPed alloy, and AZ31 reinforced with ZnO nanocomposites. The grain refinement is a process to increase

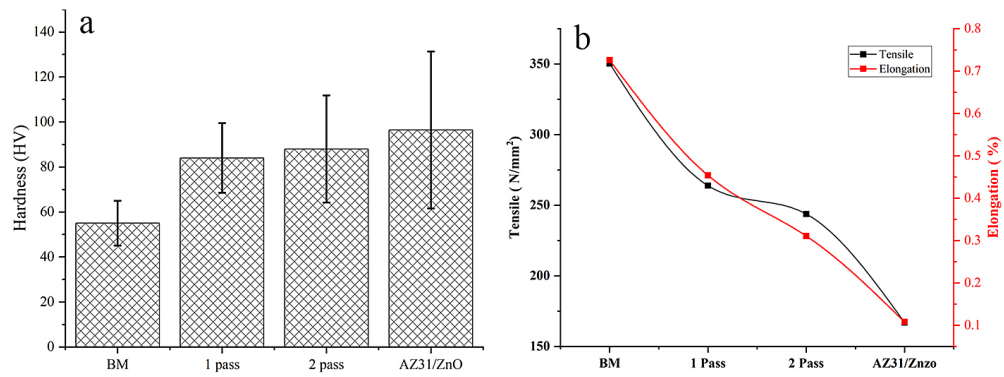


Figure 8. Hardness and tensile test results (a) microhardness for (BM, 1 pass, 2 passes, AZ31/ZnO), (b) tensile strength for samples (BM, 1 pass, 2 passes, AZ31/ZnO)

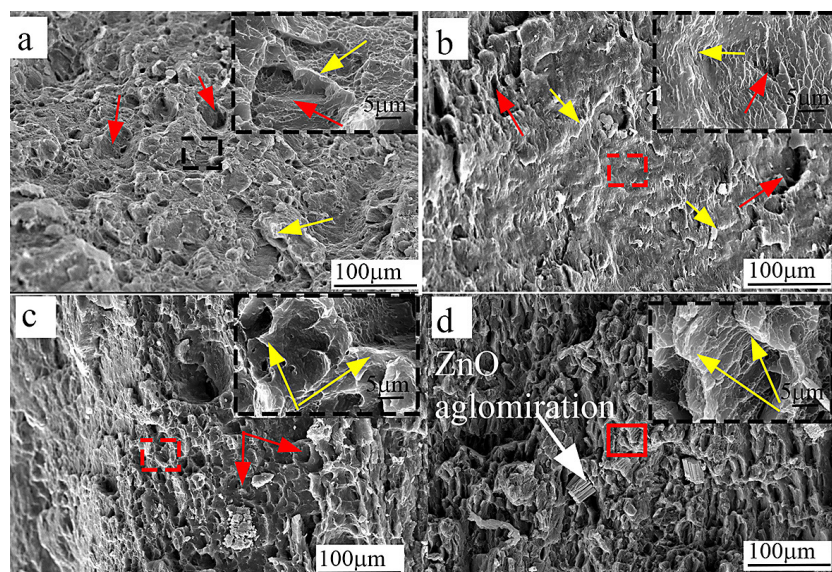


Figure 9. SEM of the fracture surface (a) AZ31 alloy matrix, (b) 1 pass FSPed AZ31 (c) 2 pass FSPed AZ31, and (d) AZ31/ZnO composite processed via 2 pass FSP

the hardness. The AZ31 hardness increased from 54 HV for an extruded alloy and recorded 84 and 88 HV for the processed AZ31 FSPed with 1 pass and 2 pass respectively. The addition of ZnO with 2 passes of FSP increased the average hardness to 96 HV for the fabricated samples. The refinement of grains (1 pass and 2 pass) and the reinforcement process improved the base alloy by 55%, 67%, and 77%, respectively. This finding is consistent with reports by other researchers. It appears that the grain size reduction was due to DRX through the FSP process[42, 47]. However, the FSP with the ZnO MMCs more effectively decreased the grain size of the AZ31 matrix, as depicted previously in Figure 6. It is believed that the ZnO nanopowder's pinning effect slowed down the grain growth of the AZ31 matrix. The

fine grain seems to be very useful for enhancing the mechanical properties, and also attractive for the low-temperature superplasticity of the magnesium alloys [2, 48].

The recent findings support previous research indicating the importance of conducting tensile tests on Mg-based alloys as biomaterials. These tests help to establish a connection between the mechanical properties and corrosion characteristics, particularly the degradation rate. The results of the tensile tests for dog bone sample with gage length 20 mm show that when nanomaterials are added to AZ31 alloys, the tensile strength decreases due to brittle ceramic material additives. On the other hand, the basic alloy exhibits a higher tensile strength due to the ductility of the base material (Figure 8b). However; the presence of

ZnO nano particle at different layers of AZ31 may be beneficial during the degradation of Mg in implanted biomatrix; where ZnO is a drug delivery that can be useful in degradation process in SBF environment [49]. Figure 9 demonstrates the fracture of the tensile samples (BM, 1 pass, 2 passes, and AZ31/ZnO). The refining of the grains via FSP changed the fracture to ductile behavior. It was observed that the fracture surface is characterized by the presence of voids in different sizes also deep dimples. The dimples (red arrow) decreased and the bright, reflective facet increased (yellow arrow) (Figure 9a-c). It can be attributed to the high strain rate on the grains and the motion of dislocation to the grain boundaries where the energy increases due to the FSP. The fracture of the ZnO/ AZ31 surface composite exhibited two types of fracture (Figure 9d), cleavage mode in the outer layer of ZnO due to agglomeration of nano ZnO particles which encourages the brittle fracture, and ductile fracture in the internal alloy under ZnO layer in FSP AZ31.

CONCLUSIONS

In this work, the surface of the magnesium alloy AZ31 was treated with FSP and ZnO nanocomposite. Two FSP passes were used to successfully manufacture the AZ31/ZnO surface nanocomposite. Following an analysis of the nanocomposite's microstructure, microhardness, tensile strength, and corrosion behavior. The following results are drawn:

1. According to microstructural studies, FSP significantly refines grain. The addition of ZnO nanoparticles and an increase in the pass number intensified the refining process to the point that, after two FSP passes the nanocomposite's average grain size dropped and the nanoparticles were evenly distributed throughout the AZ31.
2. The finer Mg grains that are intrinsic to the composite and the finely distributed ZnO particles, corrosion enhancement was attained in the AZ31/ZnO nanocomposite by reducing corrosion rate by 51% upon using the FSP and the formation of a passive film of corrosion product.
3. The hardness is significantly increased by FSP with 1 pass and 2 pass without the addition of ZnO nanoparticles. However, by using ZnO nanoparticles and raising the FSP pass number, the sample's hardness measurements improved dramatically, rising to about 77%.

4. It was observed that the fracture surface of the tensile sample was ductile fracture which is characterized by the presence of voids in different sizes also deep dimples, while the fracture surface of AZ31/ ZnO surface composite exhibited two types, cleavage and ductile fractures.

REFERENCES

1. Tan J, Ramakrishna S. Applications of magnesium and its alloys: A review. *Applied Sciences*. 2021; 11(15):6861. <https://doi.org/10.3390/app11156861>
2. Zhang J, Miao J, Balasubramani N, Cho DH, Avey T, Chang C-Y, Luo AA. Magnesium research and applications: Past, present and future. *Journal of Magnesium and Alloys* 2023. <https://doi.org/10.1016/j.jma.2023.11.007>
3. Huang Y, Zhang Y, Song J, Pan F, Willumeit-Römer R, Kainer KU, Hort N. Development and prospects of degradable magnesium alloys for structural and functional applications in the fields of environment and energy. *Journal of Magnesium and Alloys* 2023. <https://doi.org/10.1016/j.jma.2023.09.013>
4. Reza Kashyzadeh K, Amiri N, Maleki E, Unal O. A critical review on improving the fatigue life and corrosion properties of magnesium alloys via the technique of adding different elements. *Journal of Marine Science and Engineering*. 2023;11(3):527. <https://doi.org/10.3390/jmse11030527>
5. Nie JF, Shin KS, Zeng ZR. Microstructure, deformation, and property of wrought magnesium alloys. *Metallurgical and Materials Transactions A*. 2020;51:6045–109. <https://doi.org/10.1007/s11661-020-05974-z>
6. Li D, Dai D, Xiong G, Lan S, Zhang C. Composite nanocoatings of biomedical magnesium alloy implants: advantages, mechanisms, and design strategies. *Advanced Science*. 2023;10(18):2300658. <https://doi.org/10.1002/advs.202300658>
7. Nie KB, Wang XJ, Deng KK, Hu XS, Wu K. Magnesium matrix composite reinforced by nanoparticles—a review. *Journal of Magnesium and Alloys*. 2021;9(1):57–77. <https://doi.org/10.1016/j.jma.2020.08.018>
8. Majumdar JD, Chandra BR, Nath A, Manna I. Compositionally graded SiC dispersed metal matrix composite coating on Al by laser surface engineering. *Materials Science and Engineering: A*. 2006;433(1–2):241–50. <https://doi.org/10.1016/j.msea.2006.06.105>
9. Yun E, Lee K, Lee S. Correlation of microstructure with high-temperature hardness of (TiC, TiN)/Ti–6Al–4V surface composites fabricated by high-energy electron-beam irradiation. *Surface and*

- Coatings Technology. 2005;191(1):83–9. <https://doi.org/10.1016/j.surfcoat.2004.02.040>
10. Kang H-K, Kang SB. Thermal decomposition of silicon carbide in a plasma-sprayed Cu/SiC composite deposit. *Materials Science and Engineering: A*. 2006;428(1–2):336–45. <https://doi.org/10.1016/j.msea.2006.05.054>
 11. Wang Y, Zhang X, Zeng G, Li F. Cast sinter technique for producing iron base surface composites. *Materials & Design*. 2000;21(5):447–52. [https://doi.org/10.1016/S0261-3069\(00\)00036-4](https://doi.org/10.1016/S0261-3069(00)00036-4)
 12. Ding W, Jiang H, Zeng X, Li D, Yao S. The surface modified composite layer formation with boron carbide particles on magnesium alloy surfaces through pulse gas tungsten arc treatment. *Applied Surface Science*. 2007;253(8):3877–83. <https://doi.org/10.1016/j.apsusc.2006.08.015>
 13. Raja R, Shanmugam R, Jannet S, Kumar GV, Venkateshwaran N, Naresh K, Ramoni M. Development of Al-Mg₂Si alloy hybrid surface composites by friction stir processing: mechanical, wear, and microstructure evaluation. *Materials*. 2023;16(11):4131. <https://doi.org/10.3390/ma16114131>
 14. Zulkfli Z, Hamedon Z, Fatchurrohman N. Surface modification on magnesium alloys' hardness and microstructure using friction stir processing – A review. *Jurnal Teknologi*. 2023;13(1):39–45. <https://doi.org/10.35134/jitekin.v13i1.91>
 15. Bharti S, Ghetiya ND, Patel KM. A review on manufacturing the surface composites by friction stir processing. *Materials and Manufacturing Processes*. 2021;36(2):135–70. <https://doi.org/10.1080/10426914.2020.1813897>
 16. Li K, Liu X, Zhao Y. Research status and prospect of friction stir processing technology. *Coatings*. 2019;9(2):129. <https://doi.org/10.3390/coatings9020129>
 17. Węglowski MS. Friction stir processing—State of the art. *Archives of Civil and Mechanical Engineering*. 2018;18(1):114–29. <https://doi.org/10.1016/j.acme.2017.06.002>
 18. Krishnan R, Pandiaraj S, Muthusamy S, Panchal H, Alsoufi MS, Ibrahim AMM, Elsheikh A. Biodegradable magnesium metal matrix composites for biomedical implants: synthesis, mechanical performance, and corrosion behavior – a review. *Journal of Materials Research and Technology*. 2022;20:650–70. <https://doi.org/10.1016/j.jmrt.2022.06.178>
 19. Chen L, Guo C, Blawert C, Yang J, Chen D, Wang X, Yu Z, Zheludkevich ML, Li W. Evaluation of the biodegradation product layer on Mg-1Zn alloy during dynamical strain. *Journal of Magnesium and Alloys*. 2021;9(5):1820–33. <https://doi.org/10.1016/j.jma.2021.07.002>
 20. Morisada Y, Fujii H, Nagaoka T, Fukusumi M. MWCNTs/AZ31 surface composites fabricated by friction stir processing. *Materials Science and Engineering: A*. 2006;419(1–2):344–8. <https://doi.org/10.1016/j.msea.2006.01.016>
 21. Chang C, Du X, Huang J. Achieving ultrafine grain size in Mg–Al–Zn alloy by friction stir processing. *Scripta Materialia*. 2007;57(3):209–12. <https://doi.org/10.1016/j.msea.2006.01.016>
 22. Azizieh M, Kokabi AH, Abachi P. Effect of rotational speed and probe profile on microstructure and hardness of AZ31/Al₂O₃ nanocomposites fabricated by friction stir processing. *Materials & Design*. 2011;32(4):2034–41. <https://doi.org/10.1016/j.matdes.2010.11.055>
 23. Liu Q, Ma Q-x, Chen G-q, Cao X, Zhang S, Pan J-l, Zhang G, Shi Q-y. Enhanced corrosion resistance of AZ91 magnesium alloy through refinement and homogenization of surface microstructure by friction stir processing. *Corrosion Science*. 2018;138:284–96. <https://doi.org/10.1016/j.corsci.2018.04.028>
 24. Abbasi M, Bagheri B, Dadaei M, Omidvar H, Rezaei M. The effect of FSP on mechanical, tribological, and corrosion behavior of composite layer developed on magnesium AZ91 alloy surface. *The International Journal of Advanced Manufacturing Technology*. 2015;77:2051–8. <https://doi.org/10.1007/s00170-014-6577-x>
 25. Abbasi M, Abdollahzadeh A, Omidvar H, Bagheri B, Rezaei M. Incorporation of SiC particles in FS welded zone of AZ31 Mg alloy to improve the mechanical properties and corrosion resistance. *International Journal of Materials Research*. 2016;107(6):566–72. <https://doi.org/10.3139/146.111369>
 26. Asadi P, Faraji G, Masoumi A, Besharati Givi M. Experimental investigation of magnesium-base nanocomposite produced by friction stir processing: effects of particle types and number of friction stir processing passes. *Metallurgical and Materials Transactions A*. 2011;42:2820–32. <https://doi.org/10.1007/s11661-011-0698-8>
 27. Kondaiah V, Pavanteja P, Khan PA, Kumar SA, Dumpala R, Sunil BR. Microstructure, hardness and wear behavior of AZ31 Mg alloy–fly ash composites produced by friction stir processing. *Materials Today: Proceedings*. 2017;4(6):6671–7. <https://doi.org/10.1016/j.matpr.2017.06.441>
 28. Stojadinović S, Tadić N, Radić N, Grbić B, Vasilić R. MgO/ZnO coatings formed on magnesium alloy AZ31 by plasma electrolytic oxidation: Structural, photoluminescence and photocatalytic investigation. *Surface and Coatings Technology*. 2017;310:98–105. <https://doi.org/10.1016/j.surfcoat.2016.12.073>
 29. Stojadinović S, Tadić N, Radić N, Stojadinović B, Grbić B, Vasilić R. Synthesis and characterization of Al₂O₃/ZnO coatings formed by plasma

- electrolytic oxidation. *Surface and Coatings Technology*. 2015;276:573–9. <https://doi.org/10.1016/j.surfcoat.2015.06.013>
30. Jalilvand MM, Mazaheri Y, Heidarpour A, Roknian M. Development of A356/Al₂O₃+ SiO₂ surface hybrid nanocomposite by friction stir processing. *Surface and Coatings Technology*. 2019;360:121–32. <https://doi.org/10.1016/j.surfcoat.2018.12.126>
 31. Xiong HM. ZnO nanoparticles applied to bioimaging and drug delivery. *Advanced Materials*. 2013;25(37):5329–35. <https://doi.org/10.1002/adma.201301732>
 32. Saha N, Dubey AK, Basu B. Cellular proliferation, cellular viability, and biocompatibility of HA-ZnO composites. *Journal of Biomedical Materials Research Part B: Applied Biomaterials*. 2012;100(1):256–64. <https://doi.org/10.1002/jbm.b.31948>
 33. Liu S, Paidar M, Ojo OO, Poková MŠ, Mehrez S, Zain AM, Zhao Q, Wang J. Friction stir processing of hybridized AZ31B magnesium alloy-based composites by adding CeO₂ and ZrO₂ powders: mechanical, wear, and corrosion behaviors. *Journal of Materials Research and Technology*. 2023;24:1949–72. <https://doi.org/10.1016/j.jmrt.2023.03.028>
 34. Sharma V, Prakash U, Kumar BM. Surface composites by friction stir processing: A review. *Journal of Materials Processing Technology*. 2015;224:117–34. <https://doi.org/10.1016/j.jmatprotec.2015.04.019>
 35. Mazaheri Y, Jalilvand MM, Heidarpour A, Jahani AR. Tribological behavior of AZ31/ZrO₂ surface nanocomposites developed by friction stir processing. *Tribology International*. 2020;143:106062. <https://doi.org/10.1016/j.triboint.2019.106062>
 36. Akramifard H, Shamanian M, Sabbaghian M, Esmailzadeh M. Microstructure and mechanical properties of Cu/SiC metal matrix composite fabricated via friction stir processing. *Materials & Design (1980–2015)*. 2014;54:838–44. <https://doi.org/10.1016/j.triboint.2019.106062>
 37. Abbas S, Al-Ezzi S, Albusalih D, Abdullah IT, Al-Bhadle B. The effect of FSW rotation and travel speed on corrosion behaviour of 6061-T6 welded joint. *AIP Conference Proceedings*. 2024;3002(1). <https://doi.org/10.1063/5.0205976>
 38. Huang S-J, Subramani M, Borodianskiy K. Strength and ductility enhancement of AZ61/Al₂O₃/SiC hybrid composite by ECAP processing. *Materials Today Communications*. 2022;31:103261. <https://doi.org/10.1016/j.mtcomm.2022.103261>
 39. Subramani M, Tzeng Y-C, Tseng L-W, Tsai Y-K, Chen G-S, Chung C-Y, Huang S-J. Hot deformation behavior and processing map of AZ61/SiC composites. *Materials Today Communications*. 2021;29:102861. <https://doi.org/10.1016/j.mtcomm.2021.102861>
 40. Tam KJ, Vaughan MW, Shen L, Knezevic M, Karaman I, Proust G. Modelling dynamic recrystallisation in magnesium alloy AZ31. *International Journal of Plasticity*. 2021;142:102995. <https://doi.org/10.1016/j.ijplas.2021.102995>
 41. Niu W, Wang D, Wang G, Li J. Recrystallization and Anisotropy of AZ31 Magnesium alloy by asynchronous rolling. *Metals*. 2023;13(9):1631. <https://doi.org/10.3390/met13091631>
 42. Abbass MK, Baheer NA, editors. Effect of SiC particles on microstructure and wear behavior of AA6061-T6 aluminum alloy surface composite fabricated by friction stir processing. *IOP Conference Series: Materials Science and Engineering*; 2020: IOP Publishing. <https://doi.org/10.1088/1757-899X/671/1/012159>
 43. ASTM. Standard Practice for Calculation of Corrosion Rates and Related Information from Electrochemical Measurements. USA2015. <https://doi.org/10.1520/G0102-89R15E01>
 44. Jayasathyakawin S, Ravichandran M, Ismail SO, Veerappan G. Effects of ZnO addition on the microstructure/corrosion, wear and mechanical properties of sintered Mg-Al matrix composites. *Journal of Alloys and Compounds*. 2023;958:170500. <https://doi.org/10.1016/j.jallcom.2023.170500>
 45. Hanna A, Dakhouche A, Tirsatine K, Sari A, Khereddine Y, Bradai D, Azzeddine H. Effect of hot rolling on the corrosion behavior of AZ31 magnesium alloy. *Metallurgical Research & Technology*. 2019;116(1):109. <https://doi.org/10.1051/metal/2018041>
 46. Aung NN, Zhou W. Effect of grain size and twins on corrosion behaviour of AZ31B magnesium alloy. *Corrosion Science*. 2010;52(2):589–94. <https://doi.org/10.1016/j.corsci.2009.10.018>
 47. Jlood KK, Abbass MK, Hanoon MM. Effect of Friction stir processing parameters on microstructure and mechanical properties of aluminum alloy AA6061-T6: Experimental and statistical study. *Salud, Ciencia y Tecnología-Serie de Conferencias*. 2024(3):862.
 48. Zhang Y-M, Chen L-Y, Lu S, Zhao C, Wang Y-H. Refined microstructure and enhanced hardness in friction stir-welded AZ31 magnesium alloy induced by heat pipe with different cooling liquid. *Metals*. 2019;9(11):1227. <https://doi.org/10.3390/met9111227>
 49. Azeem MA, Kumar AM, Abdelaal AF, Hussein MA. Processing, mechanical, corrosion, and wear behavior of ZnO-reinforced Mg and Mg-Zr matrix composites for bioimplant applications. *Materials Chemistry and Physics*. 2024;314:128884. <https://doi.org/10.1016/j.matchemphys.2024.128884>